Available online at www.sciencedirect.com
ScienceDirect
Journal of Nuclear Materials 356 (2006) 287–299
journal of nuclear materials
www.elsevier.com/locate/jnucmat

Irradiation conditions of ADS beam window and implications for window material

P. Vladimirov *, A. Möslang

Forschungszentrum Karlsruhe, Institut für Materialforschung I, Hermann-von-Helmholtz-Platz 1, 76344 Eggenstein-Leopoldshafen, Germany

Abstract

Accelerator driven systems (ADS) are aimed at incineration of long living radioactive isotopes of spent nuclear reactor fuel, thus providing a solution for nuclear waste utilization. The idea is to couple a subcritical nuclear reactor with a high-energy proton accelerator. Protons interacting with the liquid metal target inside the reactor will produce neutrons with energy sufficient to transform long living fuel isotopes to those with shorter decay time. In some design variants a proton beam guide and window separate the vacuum of the accelerator from the liquid metal target. The window appears to be the most critical component of the whole facility as besides liquid metal corrosion it undergoes irradiation damage from incident protons, from protons and neutrons produced by spallation inside the target as well as from fission neutrons generated in the reactor fuel assemblies. In the present work we have evaluated irradiation conditions of the ADS beam window using Monte Carlo neutron, photon and charged particle transport code MCNPX. The code and the detailed geometric model of the experimental ADS (XADS) facility allow a realistic simulation of the spallation process and transport of generated nucleons as well as evaluation of various damage and operational characteristics like displacement damage, heat deposition, gas and spallation element production rates. Present results based on the reduced beam parameters provide a hope that apart from the liquid metal corrosion (not considered in the present paper) the window material could sustain full operation during the period of 3–4 month between replacements. These results may allow reconsideration of pro and contra of the window and the windowless XADS concepts.

1. Introduction

The selection of materials able to sustain intense radiation and environmental conditions is one of the major tasks for the design of any nuclear facility. This problem appears to be specifically important for the design of an accelerator driven system for nuclear waste incineration.

Accelerator driven system (ADS) is a coupling of a subcritical nuclear reactor, which is loaded with spent nuclear fuel, with a proton accelerator. High-energy protons impinge on a liquid metal target and produce through spallation reaction large amount of high-energy neutrons, which are used for transmutation ('burning') of long-living nuclear isotopes present in the spent fuel. Such transmutations drastically reduce radio-toxicity level of the fuel

* Corresponding author. Tel.: +49 7247 82 4243; fax: +49 7247 82 4567.
E-mail address: pavel.vladimirov@imf.fzk.de (P. Vladimirov).

0022-3115/$ - see front matter © 2006 Elsevier B.V. All rights reserved.
doi:10.1016/j.jnucmat.2006.05.037

allowing storing it under special conditions for a shorter time.

Presently there are several design variants of ADS under consideration. One of the important questions to be answered is whether ADS should have a beam window separating the vacuum of the accelerator from the liquid metal target or it should be window less. Both variants have their advantages and disadvantages, however their discussion is out of the scope of the present paper. In this paper we will discuss the expected operation conditions of the ADS window and their effect on the mechanical properties of the window material.

The hot window is subjected to very high irradiation load by source protons and spallation neutrons as well as by neutrons generated inside the reactor. Selection of the material for the hot window suitable to sustain the effect of radiation for the period before the next fuel loading (about 2.5 years) without deterioration of mechanical properties presents a serious challenge for material scientists. Therefore, an assessment of irradiation conditions for the hot window is required by designers and material scientists to make the optimum and safe choice for the window material.

Ferritic–martensitic 9%Cr steel T91 is considered as a prime candidate material for the beam window.

The expected operation conditions for the ADS beam window specified in design documents [1] are summarized in Table 1.

The main task of the work consists in the evaluation of the beam window damage parameters (dpa, heat deposition, gaseous atoms and spallation element yields) and discussion of their implication to the window lifetime evaluation.

Table 1
Expected operation conditions of XADS beam window

Power released in the core	$P = 80$ MWth
Max. proton energy	$E = 600$ MeV
Max. proton beam current	$I = 6$ mA
Max. proton current density	$j < 50$ μA/cm^2
Target lifetime	About one fuel cycle (2.5 years)
Beam window lifetime	3–6 month (depending on tolerable irradiation damage to be defined)
Beam window temperature	<550 °C (to reduce thermal creep and liquid metal corrosion)

2. Calculation method

2.1. Development of XADS geometry model

In the present work we are considering a liquid metal (lead–bismuth eutectic) cooled design with the hot beam window. In this design the proton beam goes from the top of the reactor through the beam guide ended with a hemi-spherical beam window (see Fig. 1). The guide and the window tightly separate vacuum of the accelerator from the liquid lead–bismuth spallation target. High-energy neutrons and protons are initially produced via spallation reactions induced during the deceleration of the high-energy proton beam in the liquid metal target downstream the beam window. Neutrons having much larger ranges than protons reach the fuel assemblies and induce fission and transmutation of long-living radioactive isotopes.

As it follows from the design, the irradiation damage of the beam window can be subdivided into the three main components (i) source and spallation induced proton damage, (ii) spallation induced neutron damage, and (iii) fission induced neutron damage. The most critical ADS components with respect to irradiation damage and degradation of material properties are the beam window and the flow guide.

The characterization of the irradiation damage conditions for the XADS beam window requires

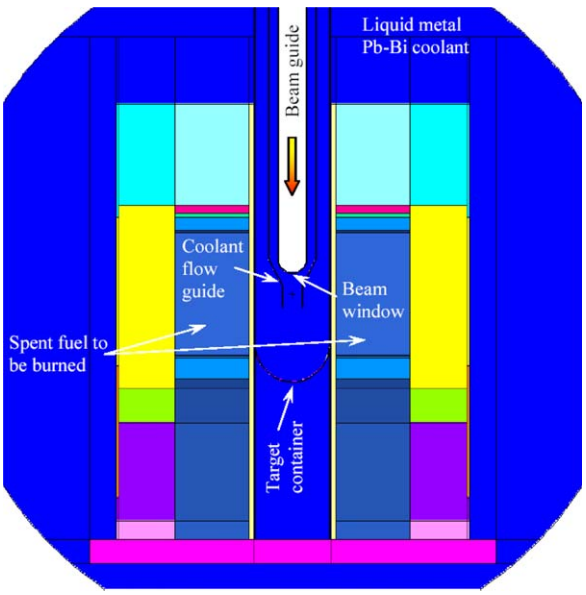

Fig. 1. XADS geometry model used for calculations. The proton beam is coming from the top.

accurate calculation of the neutron spectrum, taking into account not only a contribution from the proton beam and the neutrons produced in the liquid metal target, but also the fission neutrons coming from the fuel assemblies. To perform such an evaluation one has to rely on a geometry model adequately describing main features of the facility.

Our geometry model is based on the preliminary design developed by ANSALDO. This model (see Fig. 1) was realized as an input file for the Monte Carlo neutron-gamma-charged particle transport code MCNPX 2.1.5 [2]. For this study the thickness of the beam window was taken to be 3 mm. Previous window design optimization studies [3,4] suggested to change beam window geometry in order to minimize temperature and thermal stress gradients. It was recommended to select 2 mm thickness at the window center changing smoothly to 3 mm in the junction with the cylindrical part of the beam pipe [4]. However, the results of our calculations practically do not depend on the window thickness, as proton and neutron ranges are significantly larger.

It should be noted that due to the burnup of the fuel isotopes the criticality of the core gradually decreases with operation time from about 0.97 down to 0.94. To keep constant the thermal power released from the core (about 80 MWth in the present XADS design) the proton current should be increased continuously from about 2.5 to 5.5 mA for compensation, as analyses of the fuel burnup and criticality [5] have shown. For a given criticality level of our model a proton current of 2.78 mA was identified. The design requirements restrict the current to 6 mA and the maximum current density to 50 $\mu A/cm^2$. In accordance with recommendations from thermo-mechanical analyses [3,4], a Gaussian beam profile distribution was used for the present calculations.

2.2. Preliminary specification of irradiation conditions for the beam window

The preliminary specification of irradiation conditions for the beam window taken as initial guidelines for the XADS design as well as for material selection and qualification performed within the SPIRE project were based mainly on the calculations reported in Ref. [6]. The following parameters were used there: 365 days of irradiation with proton current density of 77 $\mu A/cm^2$ and beam energy of 1 GeV.

Since that time the beam specifications have been changed (see Table 1). In particular, the proton beam energy and current density were reduced to 20 $\mu A/cm^2$ and 600 MeV respectively.

3. Results

It should be noted that due to the reduction of the proton beam energy and current proposed by designers, the material loadings calculated in this work are considerably lower than the initial specifications mentioned above. In this section we present the results calculated with MCNPX using standard settings and the beam specifications described in Section 2.1.

Due to the nature of the MCNPX code the high and low energy particle transport is treated by separate parts of the code and the contributions of these particles to material response should be processed separately. The transport of high-energy particles (>150 MeV) was performed using nuclear models, while for the transport of low energy particles (<150 MeV) cross-section libraries have been used. The results presented below are sums of high- and low-energy contributions, if not stated otherwise.

To study the spatial dependence all material responses were calculated in a set of coaxial cylinders, subdividing the window into parts (see Fig. 4 left): inside the first cylinder ($r_1 = 1$ cm), between the first and the second ($r_2 = 2$ cm) and so on, while the radius increases each time by 1 cm.

3.1. Neutron and proton energy spectra

The spatial distribution of the proton flux calculated in the window follows the beam profile, while neutron flux is much less position dependent, because neutrons produced by spallation in the direction opposite to the proton beam are generated during transition and evaporation stages and emitted isotropically in the frame of the moving nucleus [7]. The maximum proton flux at the window center is about $F_p = 1.56 \times 10^{14}$ $p/cm^2/s$, whereas the neutron flux is one order of magnitude higher $F_n = 1.59 \times 10^{15}$ $n/cm^2/s$. This is due to the fact that in spallation reaction neutrons are emitted about 10–12 times more frequently than charged protons, which have to overcome the Coulomb barrier of the nucleus.

The energy spectrum of protons has a delta-function like contribution from the source beam and

spread-over energy contribution of the spallation-produced neutrons, which is very flat in the range 4–50 MeV (see Fig. 2).

Neutron reaction threshold energy for H and He production on iron is about 1.5 and 3.5 MeV, respectively. Hence, spallation protons could also contribute to gas production. However, the flux of incident protons is more than one order of magnitude higher (see Fig. 2), that explains why incident protons dominate the gas production rates in the beam window.

The neutron energy spectrum is broader in energy and slightly depends on the position only for energies above 1 MeV. Neutrons below 1 MeV rapidly forget the history of slowing down and have a common shape of the energy spectrum. As can be seen from Fig. 3, spallation produced neutrons have low population at high-energies.

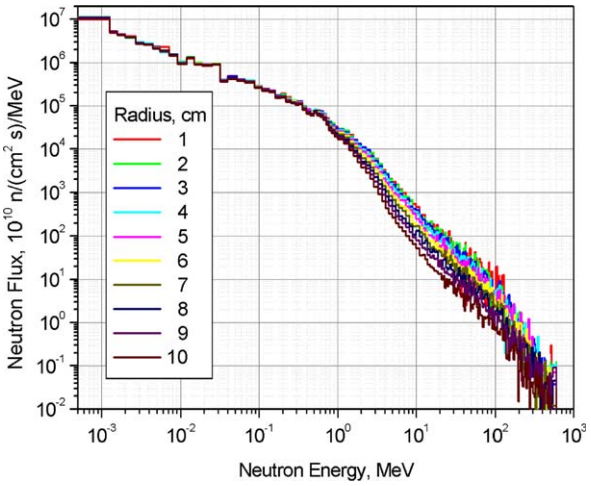

Fig. 3. Neutron energy spectrum at different positions of the beam window.

3.2. Displacement damage production rates

The neutron induced damage in the 'low-energy' region was calculated by means of MCNPX tallies using damage production cross-sections (MT = 444) from LA-150 nuclear library. The damage production was scored in a set of cylinders (with radiuses from 1 to 10 cm) subdividing the hot window (see Fig. 4). The maximum neutron induced damage accumulated inside the smaller cylinder found to be 19.4 dpa/fpy.

The contribution of the high-energy (>150 MeV) neutrons and protons to displacement damage is 12.8 dpa/fpy. About 82% of this value is due to inelastic reactions.

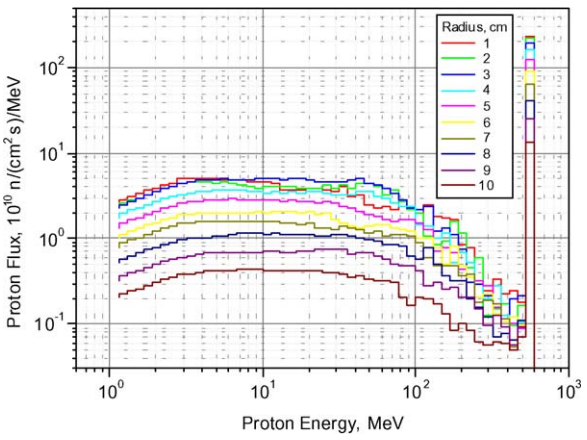

Fig. 2. Proton energy spectrum at different positions of the beam window.

The maximum total damage rate at the center of the window is about 32 dpa/fpy.

Neutrons generated by fission in the reactor core have a broad spatial distribution and produce almost constant damage of about 4.3 dpa/fpy independent of spatial position in the beam window. The contribution of fission neutrons depends on the criticality of the active core (k_{eff}) and will decrease with time due to the fuel burnup.

This is the only contribution, which scales with the core criticality. In fact, the variation of the core criticality from 0.97 to 0.94 is rather small as well as the fission neutron contribution to the total damage. Therefore, the damage production rates and all other material responses can be linearly scaled with the current density.

3.3. Gas production rates

In order to validate our gas production results calculated with MCNPX, a literature search on experimental and calculated values of gas production cross-section for iron and chromium was performed.

As was discussed in Section 3.1 the gas production cross-section values at the energy of incident protons are sufficient to estimate their contribution. However, to be able to estimate also a contribution from spallation-produced protons, a complete energy dependence of the cross-section is necessary.

Sufficiently complete energy dependence can be found only in evaluated nuclear data files. To vali-

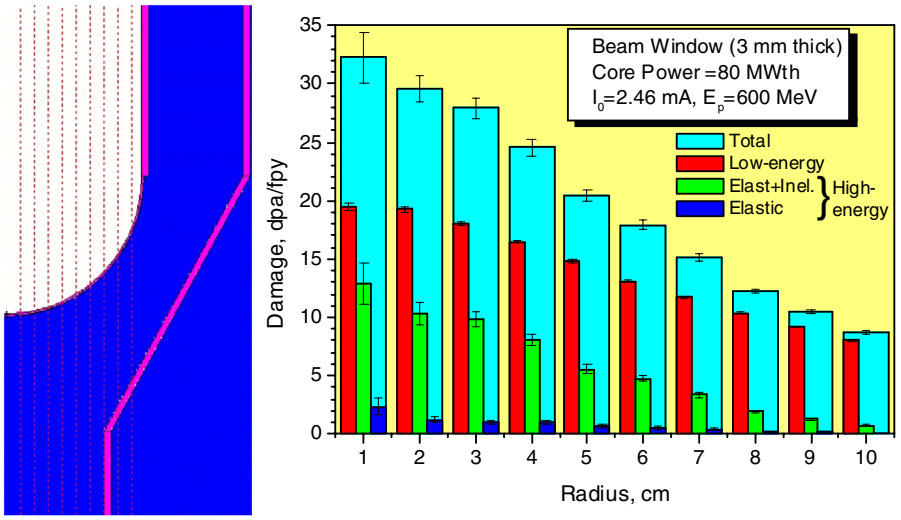

Fig. 4. Total and partial contribution to displacement damage in the beam window calculated between different coaxial cylinders as shown in the inset (left).

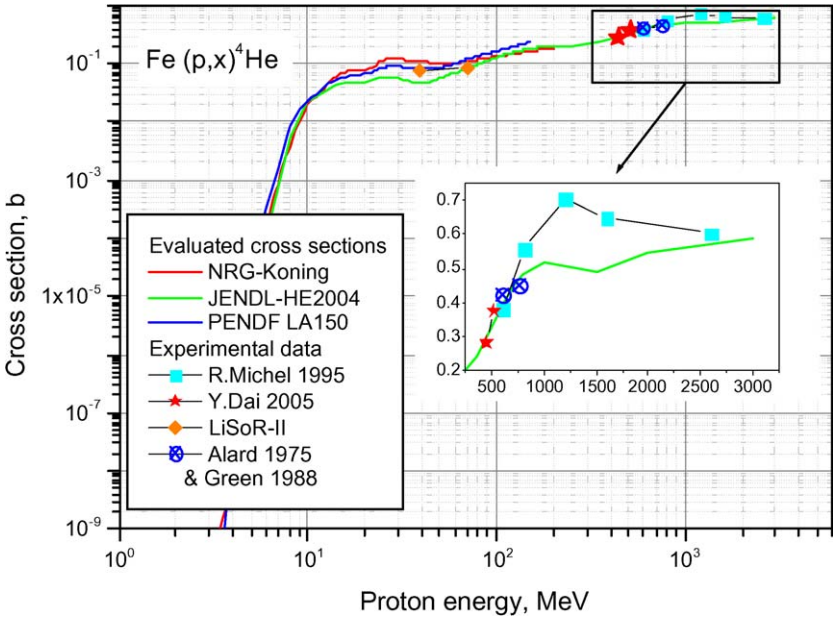

Fig. 5. Evaluated helium production cross-sections (lines) together with experimental data.

date the MCNPX results, gas production cross-sections by incident protons from LA150 [8], JENDL-HE2004 [9], NRG-2003 (A. Koning) [10] and BISERM2 [11] libraries were used together with the experimental data extracted from the PISA database (courtesy of B. Kamys) [12] and HINDAS project [13]. The only library, which covers the whole energy range up to 3000 MeV, is JENDL-High Energy File (2004).

As an example we have plotted the evaluated helium production cross-sections (see above) and several experimental data by Alard [14], Green [15], Michel [16] and more recent experiments performed at PSI [17]. Comparisons have shown that the JENDL-HE evaluation is in reasonable agreement with the available experimental data.

The spatial distribution of the total gas production in the beam window calculated with MCNPX

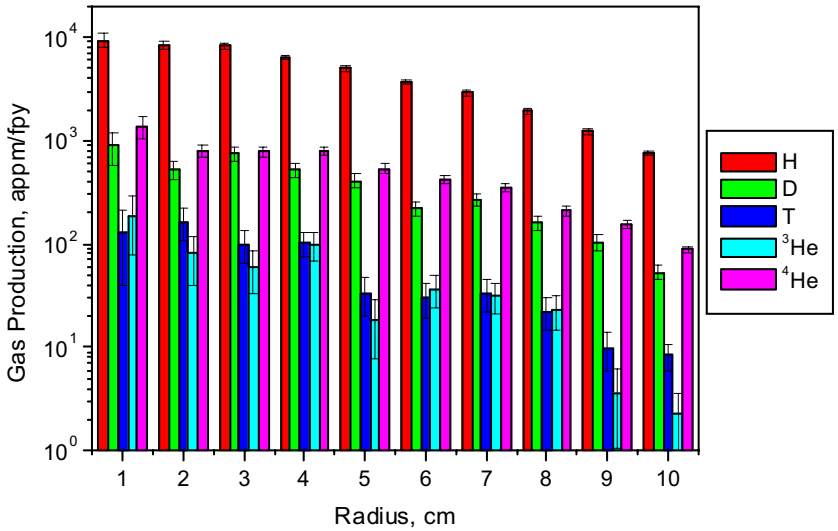

Fig. 6. Total gas production per full power year in the hot window.

is shown in Fig. 6. The major contribution to gas production is coming from the source protons, about 98% in the case of hydrogen.

The maximum gas production rates at the center of the beam window calculated by MCNPX, using JENDL-High Energy library [9] and experimental data are collected in Table 2.

3.4. Heat deposition in the beam window

The proton, gamma and neutron induced heating of the beam window (see Fig. 7) was calculated using tally suitable in the whole energy range (F6+). Nuclear models are used above the library limit of 150 MeV while heating numbers and kerma factors are exploited below. As the 600 MeV protons have a typical range of more than 10 cm, the normalized power deposition in the beam window is practically independent of window thickness variations.

It is interesting to note that the heating in the beam window is mainly due to protons. About one sixth of the total is contributed by gamma and only about 0.5% by neutrons. Due to the last fact, the heat deposition in the window is practically independent of the criticality of the active core and the results can be simply scaled with the beam current density.

The maximum heating at the center of the window is about 60 W/g (0.19 kW/cm^3/mA). This value is somewhat higher than that obtained in Ref. [18] (0.14 kW/cm^3/mA), where an elliptical beam distribution was employed. A bit lower value 0.13 kW/cm^3/mA of the maximum energy deposition density was reported in [19] for the gas cooled XADS model. The standard Bertini nuclear model was used in both cases as well as in our calculations.

As we have discussed above, the major contribution to heating is coming from the source protons. Their contribution can be estimated as

$$H[W/g] = F_p \cdot S(E_0)/\rho \cdot k,$$

where F_p and ρ stand for the proton flux and density in the cell of interest, $S(E_0)$ is a proton stopping power and $k = 1.6021 \times 10^{-13}$ is a conversion coefficient from MeV to W s. The stopping power $S(E_0)$ is

Table 2
Maximum gas production rates (appm/fpy[a]) at the center of the beam window calculated by MCNPX and using evaluated cross-section library JENDL-High Energy File 2004

	H	D	T	^{3}He	^{4}He
MCNPX (p + n)	9.3×10^3	8.9×10^2	130	180	1.4×10^3
JENDL-HE (p)	1.2×10^4	1.2×10^3	230	–	1.9×10^3
Alard [14]	1.3×10^4	1.5×10^3	230	290	2.1×10^3
Michel [16]				182 ± 13	$(1.8 \pm 0.1) \times 10^3$

[a] Here and after fpy stands for *full power year of operation*.

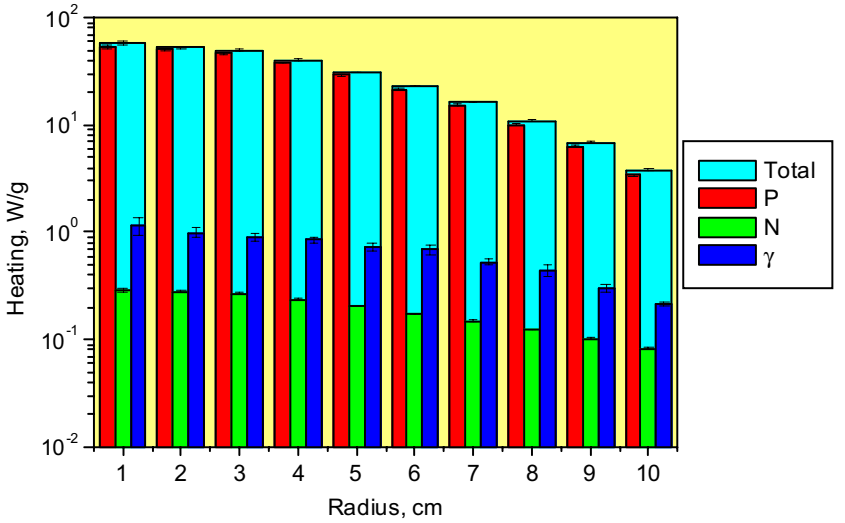

Fig. 7. Total heat deposition inside the beam window and partial contributions from protons, neutrons and gamma-rays.

mainly due to electron excitation and ionization by incident protons. In the proton energy range of interest 0.6–1.5 GeV it is a slightly decreasing function of energy and amounts to 1.8, 1.6 and 1.5 MeV/(g/cm^2) for 0.6, 1.0 and 1.33 GeV, respectively. The proton heat deposition alone estimated by the above equation for the central cylinder with $R \leqslant 1$ cm is about 51 W/g, which is close to the result obtained in [12] – 50 W/g.

3.5. Spallation product yields

Spallation reactions induced by high-energy protons and neutrons generate a huge variety of isotopes starting from the target element down to the light elements and gaseous atoms like helium and hydrogen isotopes.

In this work we have calculated the spallation element yields averaged over the whole beam

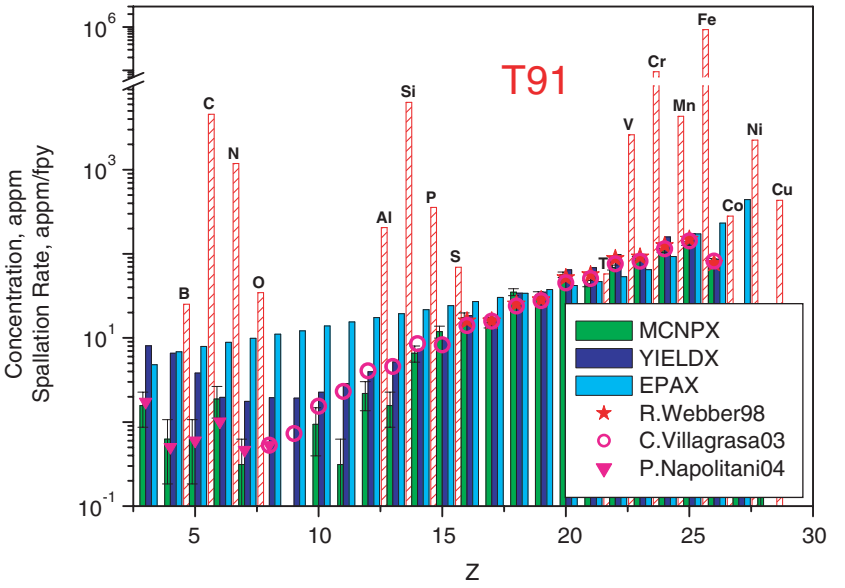

Fig. 8. Spallation element production in the beam window after 1 year of irradiation as calculated with MCNPX, using two empirical formulae [21,23] and experimental cross-sections from [24–26]. The composition of T91 is shown with hatched red bars. (For interpretation of the references in colour in this figure legend, the reader is referred to the web version of this article.)

Table 3
Limits of spallation elements production in appm/fpy

Ref.	Li	Be	B	C	N	O	F	Ne	Na	Mg	Al	Si	P	S	Cl	Ar	K	Ca	Sc	Ti	V	Cr	Mn	Fe	Co
[23]														16	16	25	28	52	56	88	92	125	150	77	
[24]						0.5	0.7	1.5	2.3	4.1	4.6	8.6	8.3	14	16	24	28	45	51	76	82	115	143	82	1.0
[25]	1.7	0.5	0.6	1.0	0.5	0.5																			
Max	8.2	2.4	2.8	4.8	2.2	2.5	3.4	7.3	11	19	22	40	39	66	74	113	130	213	239	356	383	538	670	385	4.9
T91			25	0.5%	0.1%	35					205	0.6%	357	69						58	0.3%	9.4%	0.4%	Bal.	282
			B	C	N	O					Al	Si	P	S						Ti	V	Cr	Mn		Co

window volume using standard MCNPX settings with the Bertini–Dresner model. The results are shown in Fig. 8 where MCNPX calculated yields are compared with those obtained by semi-empirical formulas YIELDX [20,21] and EPAX [22]. The calculated results obtained for the residual close to the target nuclei ($\Delta Z/Z_{\text{target}} \leqslant 40\%$) agree well with each other as well as with the results calculated using experimentally measured cross-sections [23]. In the case of light residues both formulae overestimate calculated results, while YIELDX gives closer values to those of MCNPX.

Recent experimental data [24] show excellent agreement with MCNPX results down to $Z = 14$ (Si). To obtain an estimate of spallation element production at lower atomic numbers we scaled the data measured at 1 GeV [25] to match the oxygen yield at 600 MeV [24]. The data scaled in this way present an upper limit because the light element production was not detected at 500 MeV, but already exists at 750 MeV. The MCNPX results agree within statistical errors with the limits for atomic numbers less than eight, while for Z in the range 8–13 they are somewhat below the experimental values.

Therefore, in spite of the initial concerns (see Section 2.2), the production of spallation elements appears to be not so high as it was expected initially. The results of our calculations were confirmed by recent experimental data [24,25] and can be used together as a new specification of spallation element production in the beam window.

However, the spallation element production rates are higher at the window center as compared to the values averaged over the whole window volume. The maximum rates can be estimated by multiplying the values from Table 3 by the corresponding proton flux ratio, which in our case is about 4.7. The annual production of sulfur obtained this way is close to its initial content in T91, while titanium and cobalt yields slightly surpass it. So we expect to have about 135 appm S, 400 appm P and 400 appm Ti at the window center after one year of full power operation. The consequences for the material properties are discussed in Section 4.1.

4. Discussion

The calculations of the irradiation loading characteristic for the ADS beam window have been performed in the previous part of the paper. Here we

discuss some general implications for the window material and the window design.

9–12%Cr–MoVNb steels like T91, EM10, EM12 and DIN1.4914 have been used worldwide in a variety of prototype and commercial fast breeder reactor applications, for such heavily irradiated reactor parts as pressure tubes, sleeves, super- heaters, fuel pin cladding and wrappers or ducts. Ferritic–martensitic steels of this class are known for their excellent mechanical properties combining high temperature strength and creep resistance with high thermal fatigue life, as well as with good thermal conductivity, weldability, and resistance to corrosion [26]. Amongst these the modified T91, containing 9Cr–1Mo with small additions of V and Nb, favorably compares with austenitic grades, because of its better long term creep and creep-rupture properties up to 550 °C. In addition this steel class has not only demonstrated safe and reliable operation up to high displacement damage doses of 150–200 dpa, but also has shown superior irradiation swelling resistance and excellent thermo-physical properties at elevated temperatures [27,28]. However, since the introduction of ferritic–martensitic steels in reactor irradiation programs it become also clear that besides limitations in the long-term creep strength beyond about 550 °C, commercial 9–12%Cr–MoVNb steels show substantial irradiation induced hardening below ~420 °C with a related severe degradation of fracture toughness and ductility. While above ~450 °C there is no irradiation induced hardening at all. The main reason for the severe irradiation hardening and the related material degradation are point defect clusters and interstitial type loops that are no longer stable above ~420 °C.

In addition to these dpa dominated irradiation effects, fusion neutrons and even more spallation sources like ADS produce orders of magnitude higher rates of *gaseous transmutations* (He and hydrogen isotopes) and *spallation isotopes* (e.g. P, S, Ca), than any fission reactor. As these gaseous and spallation elements intrinsically interact with displacement damage induced defects (e.g. cascades and point defect clusters), they can severely accelerate the irradiation-induced degradation of macroscopic observables. Some examples highlighting these effects are outlined in the following in order to select the most appropriate temperature window and to evaluate briefly some design limits of the T91-type steel class.

4.1. Operational temperature range for the beam window material

The optimal temperature range for the beam window material is restricted by irradiation induced hardening at temperatures below 420 °C and, from the other side, by significant strength reduction, thermal and irradiation enhanced creep and high temperature helium embrittlement at temperatures above 550 °C. Using of reduced activation oxide dispersion strengthened steels developed recently for fusion applications [29] could probably expand the temperature window to at least 650 °C.

The maximum temperature of the outer surface contacting liquid metal should not exceed 500 °C, to avoid significant liquid metal corrosion of the window material. Both requirement were fulfilled by the modified design of the window: the window thickness gradually changes from 3 mm at connection with the beam guide to 2 mm at the window center [30].

4.2. Spallation element induced embrittlement

Long-term experience in fission reactors has shown that elements like phosphorous and sulfur often accelerate irradiation embrittlement even at very low concentrations due to their pronounced segregation at grain boundaries. In addition to that some elements tend to cluster and precipitate in the bulk of grains. Calcium and sulfur with their very low solubility are, among other spallation products, good candidates for clustering and precipitation.

The effect of alloying elements like Ti, P and S on the microstructure and mechanical properties of 9% Cr ferritic–martensitic steels was investigated in the frame of the EU SPIRE project. Testing of the impact properties has shown the reduction of ductility for all doped samples [31]. The doping concentrations (0.2–0.25 wt% Ti, 400 appm S, 300 appm P) were considerably higher than the yields per year presented in this paper (see Table 3), except phosphorous, which doping concentration was slightly lower. The sample doped with all three impurities showed fourfold decrease in the upper shelf energy and the ductile–brittle transition temperature (DBTT) around +40 °C. Specially purified grades of EM10 containing less alloying elements like Si, Ni, Mo, Nb and W have shown better impact properties than commercially produced T91.

Fortunately, the effect of phosphorous alone can be deduced from the results of Ref. [32], which

describes the effect of aging of 9Cr–1Mo steel at 550 °C doped with 10, 170 and 840 appm P on ductility. Linear extrapolation to the phosphorous concentration expected in the center of the window after 2400 h (110 appm P) yields a DBTT of about −27 °C. This value presents an upper limit, because in the beam window phosphorous concentration increases with a constant rate of about 1.1 appm P per day, while in the referenced experiment doping was performed before aging. So more pronounced phosphorous segregation is expected in the latter case. It follows from the extrapolation formula that DBTT increases with P concentration by approximately 3 °C per 100 appm P. On the other hand, irradiation enhanced diffusion will increase phosphorous segregation.

Ca and S clustering was not detected at 500 °C by transmission electron microscopy (TEM) even at concentrations of 1 at.% [33]. However, uniformly distributed Ca clusters with typical diameter below 2 nm, invisible for TEM, were found at 300 °C by atom probe experiments [34].

The study of the doped grades has shown that a number of stable precipitates like TiS, TiN and MnS as well as less stable (which partly dissolve at 1350 °C) as CrS and Ti(Mo)C can be observed. These precipitates seem to be mainly responsible for the poor impact properties of these materials [31].

Auger analysis of the fracture surface of tensile specimens made of doped martensitic steels has shown [35] that intergranular fracture surfaces are enriched with phosphorous and molybdenum and have somewhat higher chromium content. It is interesting to note that no evidence of sulfur segregation to the grain boundaries (GBs) was detected for doped grades of EM10 [35], while for F82H aged at 600 °C homogeneous distribution of sulfur near GB not related to sulfur precipitation was observed [36]. It seems that these results are generally consistent with the assumption of the competitive segregation of P and S revealed for ternary Fe–P–S alloys [37]. Both elements compete for sites at the GB and if the activity of either element is raised, that element will segregate more and retard segregation of the other. Activity of sulfur can be controlled with small additions of Cr or Mn, both of them are known to form sulfides. Addition of carbon or nitrogen decreases phosphorous segregation, while that of manganese increases it.

The experience in worldwide development of reduced activation ferritic martensitic steels has shown that a reduction of impurity concentrations of B, P and S to the lowest possible level could significantly reduce the tendency to embrittlement. Therefore, initially purified steels are recommended to withstand the effect of spallation elements for a longer time.

4.3. Hydrogen and helium induced embrittlement

High hydrogen production rate usually have not been considered as a dangerous factor as hydrogen practically does not retain in ferritic–martensitic steels. In fact, we have proved that the critical concentration for hydrogen embrittlement (~10 appm H for 10 wt%Cr steels [38]) cannot be reached in the window due to the high mobility of hydrogen in the range of the window operation temperatures.

Oxide layers or protective coatings, which are used to prevent window material from liquid metal corrosion, could have some detrimental effect with respect to gaseous atom trapping and retention. Some protective layers are not penetrable for gases. In this case maximum hydrogen concentration in the window would be higher by a factor of four [39], but still much lower than the critical one. Hitherto we did not consider the effect of hydrogen trapping by irradiation-induced defects and at the interface with protective layer. However, the oxide layers or coatings could potentially trap H and/or He resulting in blistering or pilling off the protective layer. Hydrogen is known to be trapped in the stress field of a crack and might be trapped in the stress field of other irradiation produced defects (like void or dislocation loop) as well. Retention of hydrogen increases brittleness of material and stimulates microcrack growth under fatigue condition.

In spite of the fact that hydrogen retention in ferritic–martensitic steels is much lower than in austenitic steels it was found that hydrogen can accumulate in irradiated ferritic–martensitic steels. For example, irradiation in SINQ revealed that the peak of hydrogen desorption in reduced activation steel F82H shifts from 290 °C at 10 dpa to 430 °C at 20.3 dpa, while the total amount of the hydrogen retained decrease with the irradiation dose [40]. In non-irradiated steels hydrogen is trapped mainly by dislocations in martensite substructure and by newly created grain boundaries in ferrite matrix [41]. In irradiated materials hydrogen is bounded with irradiation-induced defects as well. Some of the defect clusters are growing with dose and their binding energy with hydrogen increases.

That results in shifting of the hydrogen desorption peak to higher temperature.

Simultaneous irradiation by iron, helium and hydrogen ions increases swelling of 9% and 12%Cr alloys irradiated to 50 dpa at 510 °C from 0.5% for the self-ion irradiation to almost 4% in the case of triple beam irradiation [42]. It should be noted that the temperature of maximum swelling is shifted from 430 °C [43] to 510 °C in the presence of hydrogen.

Even in a typical fast breeder neutron spectrum the He gas/displacement damage ratio is below 1 appm He/dpa, while in a first wall fusion reactor spectrum this ratio is 10–12 appm He/dpa, and in the ADS demonstrator it amounts to about 50 appm/dpa (Figs. 3 and 5). Even more sensitive to the high-energy tail of the neutron spectrum is the production of hydrogen isotopes, as also shown in the preceding chapter. Fortunately, in many bcc alloys like ferritic–martensitic steels the mean free diffusion path of migrating He atoms below about 600 °C is much smaller than the typical width of lath boundaries (0.5–1 μm) or the average grain diameter (~15–30 μm). That is, in ferritic–martensitic steels the vast majority of helium remains even at high temperatures around 600 °C in the matrix as relatively small and stable equilibrium bubbles or He filled cavities, while in austenitic steel like 316LN a significant fraction of helium reaches the grain boundaries leading to the well known severe high-temperature helium embrittlement. However, at 420 °C and below, in ferritic–martensitic steels helium is trapped either at already existing defect clusters or precipitates in nm scaled bubbles. Helium bubbles are quite stable and even the cyclic motion of dislocations during post-irradiation or in-beam fatigue testing is not able to sweep the He-bubbles to boundaries [44]. From a combination of He implantations [27,44,45] with neutron irradiations after Ni-doping [46] and B-doping [47,48] it can be concluded that below about 420 °C helium concentrations up to 500 appm have the following effects: (i) hardening contribution of about 60–100 MPa which is beyond 1–3 dpa about 20% of the total irradiation induced damage, (ii) ductile to brittle fracture temperature increase of about 25 °C at lower dpa doses, and (iii) lifetime reduction of a factor of five in isothermal strain controlled fatigue tests [44].

Up to now there is no common consensus on the value of the critical helium concentration for the high temperature helium embrittlement. A value in the range of 100 appm was suggested [39] for the low temperature helium embrittlement. For temperatures higher than 400 °C and helium concentrations of 0.25 at.% only moderate hardening is observed [49]. However, it was shown in a number of publications [45,50,51] that at higher temperatures (450–550 °C) a higher critical helium concentration of 500–600 appm could be adopted. A similar value of 500 appm was obtained by analysis of small punch test results after proton irradiation at SINQ [52]. Nevertheless, more reliable value for ferritic–martensitic steels as a function of irradiation temperature should be obtained experimentally. With the maximum production rate of ~2000 appm He per year (see Section 3.3) the critical limit could be reached after 3–4 months of full-power operation. It seems that this window replacement periodicity is also acceptable with respect to spallation element accumulation.

4.4. Effect of stress and corrosion on the window lifetime

The beam window is heated by the proton beam and explores incidental temperature and thermal stress variations due to unavoidable beam trips. The number of such trips can be about 300–400 per year [53]. The transition stress analysis after the beam interruption longer than 4.5 s has shown that maximum Von Mises stress in the window made of HT9 can reach 175 MPa [54]. This stress is well below the ultimate tensile stress (UTS) of 300–450 MPa (T91 steel after normalization and tempering) expected for the window operation temperature range [31]. It should be noted that UTS decreases with irradiation dose due to irradiation induced softening at $T > 450$ °C. On the other hand helium-induced hardening usually compensates this softening. A fatigue lifetime of HT9 window was estimated from a design curve by neglecting the effect of creep as well as the effects of irradiation and helium to be 10^5 cycles [54]. However, during the shock loading microcracks can develop either inside the window material or at the surface. If the window is covered with a protective oxide layer, some of which are brittle (e.g., Cr_2O_3), a crack could start from the oxide layer and will develop fast as liquid metal penetrating inside the crack significantly decreases material cohesion at the crack tip.

5. Summary and conclusion

Based on the long term experience of material behavior under irradiation and operation temperature

of the beam window (450–550 °C) one can conclude that irradiation creep, radiation induced segregation and high temperature helium embrittlement are the most important processes resulting in degradation of mechanical properties of the beam window.

Increased annihilation of point defects results in disappearance of irradiation hardening above 420–450 °C. That is, to avoid hardening the temperature of the window should be higher than this limit.

The helium production rate taken initially as a guideline (about 5000 appm/fpy) was much higher than the present results of 2000 appm He/fpy obtained for the reduced beam parameters. The data discussed so far suggest that helium concentrations of 500–600 appm (which seems to be below the critical limit for mechanical property degradation) will be accumulated during 3–4 months of operation. This time seems to be quite acceptable for the periodical window replacement.

The following concentrations of 37 appm S, 110 appm P and 110 appm Ti are expected to accumulate at the window center during 100 days of full power operation. These concentrations seem to be acceptable with respect to reduction of tensile and impact properties. The effect of the additional elements (not contained initially in the window material) on mechanical properties should be investigated. Purification of the structural material with respect to P and S, which is a standard practice for reduced activation steel production, is recommended also for candidate ADS window steels to extend the window lifetime.

The present investigation suggests that on the basis of the reduced proton beam parameters commercial ferritic–martensitic steels (like T91) provides sufficient margins to sustain the severe operation conditions of a beam window for at least 100 days. A minimum window lifetime in this range might be sufficient to reconsider pro and contra of the window and the windowless XADS concepts.

Acknowledgements

This work was supported by the European Community within the SPIRE project by the contract FIKW-CT-2000-0058.

The authors would like to express their acknowledgements to

- Dr C. Broeders and Dr A. Konobeev (FZK/IRS) for helpful discussions and sharing their knowledge about MCNPX code.
- Dr A. Travleev (FZK/IRS) for providing homogenized geometry model for the windowless XADS design.
- Professor B. Kamys (Jagellonian University) for providing PISA database, which compiles experimental data on proton induced cross-sections in spallation region.
- Dr F. Goldenbaum (Fz Jülich) for providing reprints of his publications on damage and gas production at spallation neutron sources.
- Dr T. Fukahori (JAERI) for providing JENDL-HE2004 evaluated nuclear cross-section library.

References

[1] L. Cinotti et al., XADS Pb–Bi Cooled Experimental Accelerator Driven System – Reference Configuration – Summary Report, ANSALDO ADS1SIFX0500, Rev 0, June 2001; ANSALDO, Tech. Report 'Technical specification and target unit interfaces (LBE and gas cooled concepts, window and windowless options)', 30.10.2001, ADS 43 TIIX 010, FIKW-CT-2001-00179.
[2] L.S. Waters (Ed.), MCNPX™ Users Manual, Version 2.1.5, TPO-E83-G-UG-X-00001, Rev. 0, 14 November 1999.
[3] V. Bellucci, S. Buono, G. Fotia, L. Maciocco, V. Moreau, M. Mulas, G. Siddi, L. Sorrentino, in: Proceedings of NEA Workshop on Utilization and Reliability of High Power Accelerators, 13–15 October 1998, Mito, Japan, NEA, ISBN: 92-64-17068-5, 1999.
[4] N. Tak, H.-J. Neitzel, X. Cheng, Nucl. Eng. Des. 235 (7) (2005) 761.
[5] M.F. McDermott et al., in: Proceedings of International Workshop on P&T and ADS Development, Mol, Belgium, 2003.
[6] J. Henry, C. Volant, R. Legrain, Int. Report NT/SRMA/00-2360/DAPNIA/SPhN-00-18, May 2000.
[7] G.S. Bauer, Nucl. Instrum. and Meth. A 463 (2001) 505.
[8] M.B. Chadwick, S.C. Frankle, R.C. Little, P.G. Young, in: Proc. of the Topical Meeting on Nuclear Applications of Accelerator Technology, American Nuclear Society, La Grange Park, IL, 1997, p. 175.
[9] T. Fukahori, in: Proceedings 2001 Workshop on Nuclear Data Production and Evaluation, Pohang Accelerator Laboratory, Pohang, Korea.
[10] A.J. Koning, J.P. Delaroche, Nucl. Phys. A 713 (2003) 231.
[11] A.Yu. Konobeyev, Yu.V. Konobeev, Yu.A. Korovin, Nuclear Data to Study Damage in Materials under Irradiation by Nucleons with Energies up to 25 GeV, INPPE, Obninsk, November 2000.
[12] R. Barna et al., NIMA 519 (2004) 610.
[13] D. Filges, F. Goldenbaum, HINDAS Project WP4, Progress Report D14, September 2002.
[14] J.P. Alard et al., II Nuovo Cimento 30 (1975) 320.
[15] S.L. Green, W.V. Green, F.H. Hegedus, M. Victoria, W.F. Sommer, B.M. Oliver, J. Nucl. Mater. 155–157 (1988) 1350.
[16] R. Michel et al., Nucl. Instrum. and Meth. B 103 (1995) 183.
[17] Y. Dai, J. Nucl. Mater., these Proceedings; Y. Dai, private communication.

[18] A. Batta et al., in: Proceedings of the International Workshop on P&T and ADS Development 2003, Belgium, 6–8 October 2003.
[19] S. Cuesta et al., in: Proceedings of the International Workshop on P&T and ADS Development 2003, Belgium, 6–8 October 2003.
[20] L. Sihver, C.H. Tsao, R. Silberberg, T. Kanai, A.F. Barghouty, Phys. Rev. C 47 (1993) 1225.
[21] R. Silberberg, C.H. Tsao, A.F. Barghouty, Astrophys. J. 501 (1998) 911.
[22] K. Sümmerer, B. Blank, Phys. Rev. C 61 (2000) 034607.
[23] W.R. Webber et al., The Astrophys. J. 508 (1998) 949.
[24] C. Villagrasa et al., J. Phys. IV France 12 (2002) Pr8-63; C.Villagrasa, PhD thesis, Available from: <http://www-wnt.gsi.de/Kschmidt/DoktorArbeiten/Carmen-Villagrasa/dapnia-03-10-T.pdf>.
[25] P. Napolitani, K.-H. Schmidt, A.S. Botvina, F. Rejmund, L. Tassan-Got, C. Villagrasa, Phys. Rev. C 70 (2004) 054607.
[26] D. Laverde et al., Corros. Sci. 46 (2004) 613.
[27] K. Ehrlich, D.R. Harries, A. Möslang, Report FZKA 5626, 1997.
[28] R.L. Klueh, D.R. Harries, ASTM MOB03, 2001, ISBN 0-8031-2090-7.
[29] R. Lindau et al., Fusion Eng. Des. 75–79 (2005) 989.
[30] N. Tak, H.-J. Neitzel, X. Cheng, Nucl. Eng. Des. 235 (2005) 761.
[31] Y. de Carlan, S. Urvoy, Y. Tournie, P. Wident, NT SRMA 2581, 2004.
[32] F.W. Noble, B.A. Senior, B.L. Eyre, Acta Metal. Mater. 38 (1990) 709.
[33] G. Amiri, M.-O. Ruault, J. Henry, H. Bernas, E. Cadel, P. Pareige, J. Phys. IV France 12 (2002) Pr8-85.
[34] E. Cadel, P. Pareige, M.-O. Ruault, J. Phys. IV France 12 (2002) Pr8-93.
[35] M. Garcia-Mazario, A.M. Lancha, SPIRE Report WP2, CIEMAT DFN/ME-16/IE-04, Deliv. no. 33.
[36] J. Lapeña, M. Garcia-Mazario, P. Fernández, A.M. Lancha, J. Nucl. Mater. 283–287 (2000) 662.
[37] C.L. Briant, Acta Metal. 36 (1988) 1805.
[38] P. Jung, Fusion Tech. 33 (1998) 63.
[39] P. Jung, J. Nucl. Mater. 296 (2001) 165.
[40] B.M. Oliver et al., J. Nucl. Mater., these Proceedings, doi:10.1016/j.jnucmat.2006.05.025.
[41] F.-G. Wei, k. Tsuzaki, Scr. Mater. 52 (2005) 467.
[42] T. Tanaka et al., J. Nucl. Mater. 329–333 (2004) 294.
[43] E. Wakai et al., J. Nucl. Mater., these Proceedings, doi:10.1016/j.jnucmat.2006.05.032.
[44] R. Lindau, A. Möslang, J. Nucl. Mater. 212–215 (1994) 599.
[45] R. Lindau, A. Möslang, D. Preininger, M. Rieth, H.D. Röhrig, J. Nucl. Mater. 271–272 (1999) 450.
[46] R.L. Klueh, D.J. Alexander, J. Nucl. Mater. 187 (1992) 60.
[47] E.V. van der Osch, M.G. Horsten, G.E. Lucas, G.R. Odette, in: M.L. Hamilton, A.S. Kumar, S.T. Rosinski, M.L. Grossbeck (Eds.), Effects of Irradiation on Materials, 19th International Symposium, ASTM STP 1366, American Society for Testing and Materials, West Conshohocken, PA, 2000, p. 612.
[48] E.I. Materna-Morris, M. Rieth, K. Ehrlich, in: 19th International Symposium, ASTM STP 1366, American Society for Testing and Materials, West Conshohocken, PA, 2000, p. 597.
[49] P. Jung et al., J. Nucl. Mater. 318 (2003) 241.
[50] A. Hasegawa, H. Shiraishi, J. Nucl. Mater. 191–194 (1992) 910.
[51] R. Kasada, T. Morimura, A. Hasegawa, A. Kimura, J. Nucl. Mater. 299 (2001) 83.
[52] R. Odette, T. Yamamoto, H. Kishimoto, J.W. Rensman, P. Spatig, J. Nucl. Mater., these Proceedings, doi:10.1016/j.jnucmat.2006.05.041.
[53] Y. Dai et al., J. Nucl. Mater., these Proceedings.
[54] V. Belucci et al., in: Proceedings of the OECD Meeting, Japan, 1998.